Hindawi
Journal of Nanomaterials
Volume 2022, Article ID 1024554, 18 pages
https://doi.org/10.1155/2022/1024554

Research Article

Cadmium and Lead Removal from Aqueous Solution Using Magnetite Nanoparticles Biofabricated from *Portulaca oleracea* Leaf Extract

Payam B. Hassan,[1] **Rezan O. Rasheed**,[1] **and Kiomars Zargoosh**[2]

[1]*Department of Biology, College of Science, University of Sulaimani, Qlyasan Street, Sulaimani City, Kurdistan Region, Iraq*
[2]*Department of Chemistry, Isfahan University of Technology, Isfahan, Iran*

Correspondence should be addressed to Payam B. Hassan; payam.hassan@univsul.edu.iq

Received 13 March 2022; Revised 10 June 2022; Accepted 13 July 2022; Published 16 August 2022

Academic Editor: Haisheng Qian

Magnetic nanoparticles of iron oxide (Fe_3O_4 NPs) were prepared using a biosynthetic method to investigate their potential use as an adsorbent for adsorption of Pb(II) and Cd(II) from the aqueous solution. The present study for the first time used the magnetite nanoparticles from leaf extract of *Portulaca oleracea* for the removal of Pb(II) and Cd(II) metal ions. Characterizations for the prepared Fe_3O_4 NPs (PO-Fe_3O_4MNPs) were achieved by using X-ray diffraction (XRD), field emission scanning electron microscope (FESEM), energy-dispersive X-ray spectroscopy (EDX), transmittance electron microscopy (TEM), and Fourier transform infrared (FTIR) spectroscopy. The batch adsorption process has been performed to study the effect of various parameters, such as contact time, pH, temperature, initial metal concentration, and adsorbent dose. The optimum pH for Cd(II) and Pb(II) adsorption was 6. The removal of heavy metals was found to increase with adsorbent dosage and contact time and reduced with increasing initial concentration. Langmuir, Freundlich, Khan, and Toth isotherms were used as adsorption isotherm models. The adsorption data fitted well with the Freundlich isotherm model with correlation coefficient ($R^2 > 0.94$). The maximum adsorption capacities (Q_{max}) at equilibrium were 177.48 mg/g and 108.2267 mg/g for Cd(II) and Pb(II), respectively. The kinetic analysis showed that the overall adsorption process was successfully fitted with the pseudo-second-order kinetic model. The calculated thermodynamic parameters (ΔG°, ΔH°, and ΔS°) showed that the adsorption of Cd(II) and Pb(II) ions onto PO-Fe_3O_4MNPs was exothermic and spontaneous. These results demonstrate that biogenic synthesized PO-Fe_3O_4MNPs are highly efficient adsorbents for the removal of Pb(II) and Cd(II) ions from contaminated water.

1. Introduction

Water is the most important molecule on the earth and is a source of sustainable life. However, millions of people face water scarcity daily [1]. Rapid population growth demands a rapid expansion in the agricultural and industrial sectors, resulting in increased demand for water, which is necessary for the survival of all living forms on this blue planet [2]. Due to the release of untreated organic/inorganic harmful effluents into freshwater bodies, rapid growth in industrialization, population, and urbanization has resulted in a severe exponential increase in environmental pollution [3–5].

When water is contaminated, removing the pollutants is costly, difficult, and often impossible. Water pollution is not only harming the organisms but also destroying entire ecosystems [6, 7]. Heavy metals are well recognized among the various pollutants that contribute to environmental damage, owing to their persistence in the environment, toxicity, and bioaccumulative nature, all of which lead to negative consequences for human health and the ecosystem [8, 9]. Lead, chromium, nickel, cadmium, and arsenic in the environment pose a serious threat to plants, animals, and even humans due to their bioaccumulation, nonbiodegradability, and toxicity even at trace concentrations [10].

Human exposure to even trace concentrations may result in conditions such as cardiovascular problems, depression, gastrointestinal and renal failure, neurological damage, osteoporosis, tubular and glomerular dysfunction, and various cancers [11, 12]. Cadmium and lead are two of the most toxic metals for plants, animals, and humans. They are also harmful at low concentrations because they disrupt enzyme functioning, replace essential metals in pigments, and produce reactive oxygen species [3, 13]. As a result of these serious issues, many effective methods to remove heavy metals have been developed, including ion exchange, membrane filtration, adsorption, photodegradation, coagulation–flocculation, electrodeposition, and electrooxidations [14–18]. Until now, adsorption is the most preferred method for water purification due to its efficiency, low operational cost, and application in both small- and large-scale operations [19]. Various kinds of adsorption materials have been used for water remediation, including carbon-based materials, clays, biological materials, bentonite, zeolites, metal oxide, magnetic nanoparticles, agricultural residues, and mesoporous substances such as MCM-41, MCM-48, and SBA-15 [20, 21].

Magnetite nanoparticles (NPs) are strong adsorbents for removing pollutants from wastewater. Due to their magnetic properties, they may be easily isolated from the reaction media by applying an external magnetic field. Furthermore, the application of magnetic separation on the nanoadsorbents provides the crucial benefit of the rapid removal of toxic metals from wastewater [22].

Different methods including coprecipitation, thermal decomposition, microemulsion, and solvothermal techniques can be used to fabricate magnetite Fe_3O_4 NPs [23]. Hazardous chemicals, organometallic precursors, and hard reaction conditions, such as high pressure or high temperature, are used in these procedures. However, these methods have several disadvantages, including high toxicity, low nanoparticle stability, exhibiting low dispersion rates, and undesirable to work within scaled-up applications [24, 25]. Therefore, the fabrication of magnetite NPs by both economically and environmentally sustainable processes is necessary. The application of leaf extracts for nanoparticle synthesis has attracted a lot of attention in recent years, due to their low cost, nontoxicity, wide availability, strong metal capping affinity, biodegradability, and nonmutagenicity [26, 27]. Alcohols, aldehydes, amines, carboxyl, ketones, hydroxyl, and sulfhydryl are the intervening functional groups in the synthesis of NPs; therefore, nearly any biological substance containing these groups can be used to convert metal ions into NPs. Some molecules, such as terpenoids, flavonoids, different heterocyclic, polyphenols, reducing sugars, and ascorbate, are directly involved in the synthesis of NPs, while others, such as proteins, serve as stabilizing agents [28]. Examples of plant extracts that have been used in the biosynthesis of NPs include *Camellia sinensis*, *Quercus virginiana*, *Punica granatum*, and *Eucalyptus globulus* [24], *Moringa oleifera* [29], and *Calliandra haematocephala* [30] in the remediation of various pollutants in water.

In this study, *Portulaca oleracea* (family: Portulacaceae; common name, purslane) leaf extract was employed to synthesize magnetite Fe_3O_4 NPs. Due to the presence of various active phytochemicals such as alkaloids, phenols, flavonoids, coumarins, and terpenoids, Portulaca oleracea is commonly used in medical fields, such as drugs and medicine [31]. Only one study has investigated the preparation of Fe_3O_4 NPs using *Portulaca oleracea* leaf extract [32].

In this work, we have reported for the first time the use of magnetite Fe_3O_4 NPs from *Portulaca oleracea* leaf extract as efficient adsorbents to adsorb cadmium and lead from aqueous solutions. The Fe_3O_4 NPs were prepared successfully and characterized by X-ray diffraction (XRD), field emission scanning electron microscope (FESEM), energy-dispersive X-ray spectroscopy (EDX), transmittance electron microscopy (TEM), and Fourier transform infrared (FTIR) spectroscopy. The effect of different parameters has been studied such as pH, temperature, initial metal concentrations, adsorbent dose, and contact time. Furthermore, isotherm, kinetics, and thermodynamic studies were carried out to understand the mechanism of the adsorption of metal ions by the biofabricated Fe_3O_4 NPs.

2. Experimental Section

2.1. Materials. The leaves of *Portulaca oleracea* were obtained from the local market in Sulaymaniyah, Iraq. The chemicals: iron sulfate heptahydrate ($FeSO_4.7H_2O$) (Himedia, India), sodium hydroxide (NaOH) pellets (Merck, Germany), nitric acid (HNO_3) (Sigma Aldrich, Germany), lead nitrate ($Pb(NO_3)_2$) (Fluka), and cadmium nitrate ($Cd(NO_3)_2$) (BDH/England) were used as received without further purification. Stock solutions of lead and cadmium ions with concentrations of (1000 mg/L) were prepared by dissolving 1.598 g of lead nitrate and 2.744 g of cadmium nitrate in 200 mL of deionized water. A 10 mL concentrated HNO_3 was added to the metal ion solutions and then diluted to 1000 mL with distilled water. Solutions of HCl and NaOH (0.1–1 M) were used for pH adjustment.

2.2. Preparation of Portulaca oleracea Leaf Extract. Fresh *Portulaca oleracea* leaves were washed with tap water to remove the dirt and surface-adherent materials and then with double-distilled water. The thoroughly washed leaves were air-dried for about an hour. The dried leaves were made into small parts and heated in 500 mL of deionized water for the release of phenolic biomolecules, which rendered the solution yellow. The clear yellow filtrate which was named *Portulaca oleracea* leaf (POL) extract after cooling was preserved at 4°C for further use [33].

2.3. Synthesis of Magnetic Fe_3O_4 Nanoparticles. A simple and eco-friendly method was used to prepare magnetite Fe_3O_4 nanoparticles. In a glass beaker, a freshly prepared 0.1 M $FeSO_4$ solution (100 mL) was added to the POL extract at a volume ratio of 1 : 1 at room temperature. The pH of this mixture was increased to 11 by adding NaOH. The solution was then placed in a water bath for 60 min at 90°C. The formed black precipitate indicated the formation of magnetic Fe_3O_4 nanoparticles (PO–Fe_3O_4MNPs). The PO–Fe_3O_4MNPs were isolated using a magnet and then washed several times with deionized water and ethanol. After that,

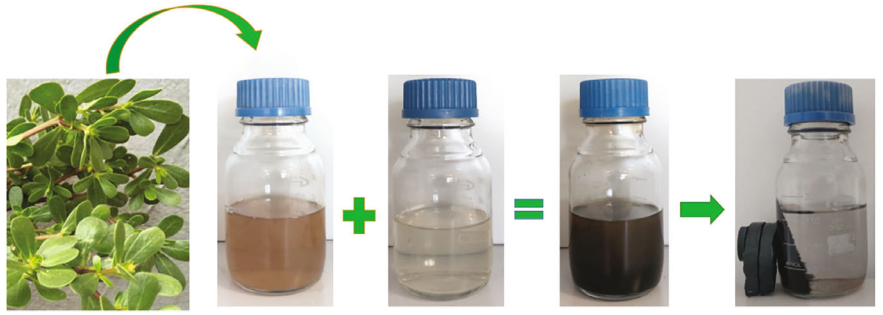

Figure 1: Biosynthesis of PO–Fe_3O_4MNPs.

the particles were dried overnight at 80°C in an air oven [30, 34]. Figure 1 illustrates a green synthesis scheme for PO–Fe_3O_4MNPs.

2.4. Characterization. An FTIR spectrometer (Thermo Scientific Nicolet iS10) was used to investigate the surface functional groups and capping agents of PO–Fe_3O_4MNPs. The crystalline structure of PO–Fe_3O_4MNPs was examined using an X-ray diffractometer (XRD) (PAN Analytical Xpert Pro, Netherlands). XRD was performed using Cu-Kα radiation ($\lambda = 1.54$ Å); the diffracted intensities of all samples were recorded in the 2θ range of 10°–80° with a step size of 0.1° and a scanning speed of 1 step/second. Field emission scanning electron microscopy (FE-SEM) (Quanta 4500, FEI) and transmission electron microscopy (TEM) (JEM-2100, JEOL, Japan) were used to examine the morphological characteristics and size of powdered PO–Fe_3O_4MNPs. The purity and the *constituent* elements of the prepared nanoparticles were confirmed by energy-dispersive X-ray spectroscopy (EDX) combined with FE-SEM.

2.5. Adsorption Tests

2.5.1. Evaluation of Optimum pH. To determine the effect of pH on the adsorption of Pb(II) and Cd(II) ions on PO–Fe_3O_4MNPs, the following procedure was used: nanosorbent (0.5 g) was added to 100 mL of 50 mg/L Cd(II) and Pb(II) solution in Erlenmeyer flasks and the pH of the solutions was adjusted from 3 to 8 using 0.1 M sodium hydroxide or nitric acid solution and agitated with a speed of 200 rpm. All the adsorption experiments were carried out at a room temperature of 20 ± 2°C. Finally, a magnet was used to separate the PO–Fe_3O_4MNPs from the solution, and the samples were filtered using Whatman filter paper (no. 1). The residual amount of Pb(II) and Cd(II) was determined by inductively coupled plasma optical emission spectrometer (ICPOES) (Optima 2100DV, PerkinElmer USA).

2.5.2. Equilibrium Contact Time. The quantity of 0.5 g of PO–Fe_3O_4MNPs was suspended separately in 100 mL of single metal ion solutions in a number of conical flasks with the concentration of 50 mg/L of Pb(II) and Cd(II). The solutions were adjusted to pH 6 and agitated with a speed of 200 rpm for different periods [35]. Ten milliliters of the sample was taken out of the flasks after 10, 20, 30, 40, 50, 60, and 70 min, and the residual Pb(II) and Cd(II) concentrations were measured using (ICPOES).

2.5.3. Effect of Initial Metal Concentrations on Adsorption. The influence of solution strength on the functional efficiency of PO–Fe_3O_4MNPs was demonstrated using different concentrations of Pb(II) and Cd(II) ions. Single metal solutions at concentrations of 10, 50, 100, and 150 mg/L in the presence of 0.5 g of PO–Fe_3O_4MNPs were agitated at a speed of 200 rpm and 20 ± 2°C for an hour [22]. After that, the magnetic nanoadsorbent was then isolated from the solution using magnets. The residual metal ion concentrations were measured using ICPOES.

2.5.4. Equilibrium Isothermal Investigation. The equilibrium adsorption isotherm is important for understanding the interaction between adsorbate and adsorbent, which provides significant information about the surface characteristics, activity of the adsorbent, and mechanism of adsorption [36]. Different amounts of PO–Fe_3O_4MNPs (0.05, 0.1, 0.2, 0.4, 0.6, 0.8, 1, 1.2, and 1.4 g) were put into a number of conical flasks. Single metal solutions at concentrations of 50 mg/L were prepared for single systems of lead and cadmium ions, respectively, and then 100 mL from each solution was added to each flask. The pH of the metal solutions was adjusted to the optimum pH value. Thermoshaker was used to agitate the solutions continuously for an hour with a speed of 200 rpm and a temperature of 20 ± 2°C. The PO–Fe_3O_4MNPs were removed from the solutions with a magnet, and the samples were filtered using Whatman filter paper (no. 1). The Pb(II) and Cd(II) concentrations in the filtrate were determined using ICPOES. The removal efficiency and adsorption capacity of PO–Fe_3O_4MNPs were calculated from experimental data using [37].

$$\%\mathrm{RE} = \frac{(C_o - C_e)}{C_o} \times 100, \quad (1)$$

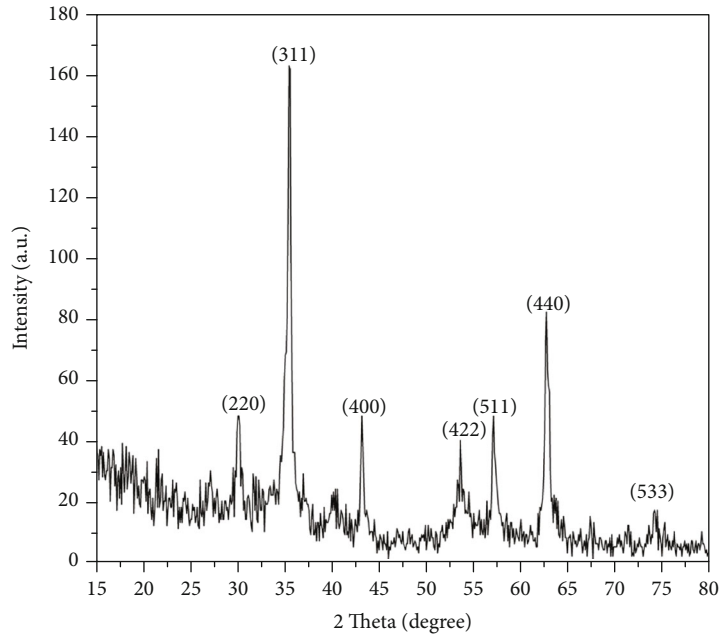

Figure 2: XRD spectra of PO–Fe_3O_4MNPs.

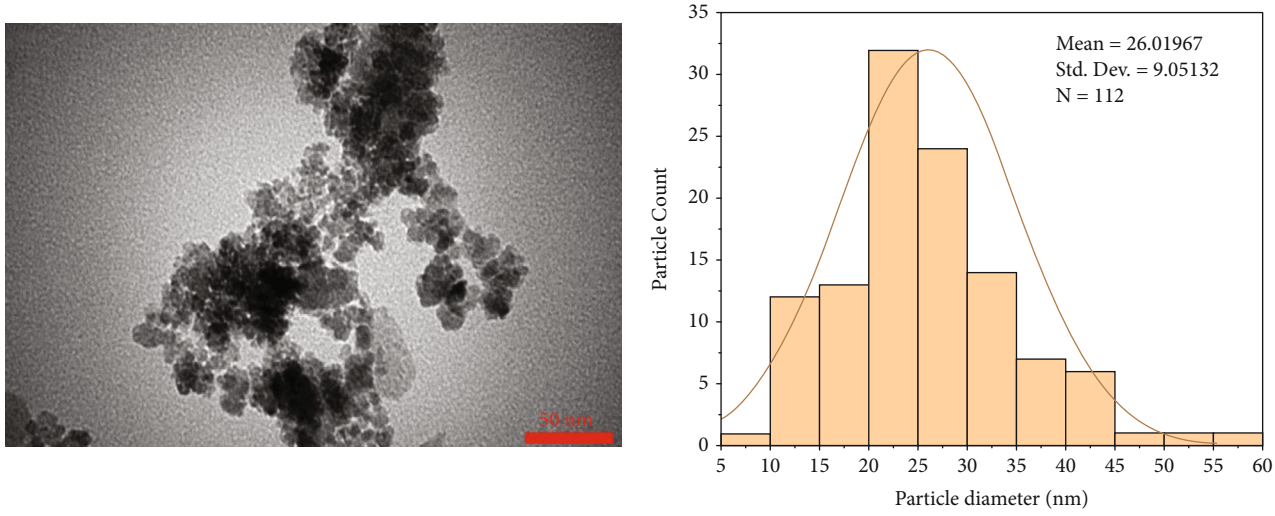

(a) (b)

Figure 3: (a) Transmission electron micrographs of PO–Fe_3O_4MNPs and (b) particle size distribution histogram.

$$q_e = \frac{V1\,(C_o - C_e)}{W_{(\text{nanosorbent})}}, \tag{2}$$

where C_o (mg/L) is the initial concentrations of metal ions Pb(II) and Cd(II); C_e (mg/L) is the equilibrium concentrations; $V1$ (L) is the volume of the metal solution, and W (g) is the dosage of PO–Fe_3O_4MNPs.

The experimental laboratory data obtained from isothermal adsorption experiments was interrelated to the common nonlinear adsorption model equations (Freundlich, Langmuir, Toth, and Khan) through the use of statistical software version 12 to compute fundamental parameters of each model. The Freundlich isotherm for heterogeneous surface energy systems is given as follows:

$$q_e = KC_e^{1/n}, \tag{3}$$

where K corresponds to the maximum binding capacity and n characterizes the affinity between the sorbent and sorbate [38].

The Langmuir adsorption isotherm which describes the adsorbate-adsorbent system equilibrium shows that all adsorbed species interact only with one site and not with each other, and adsorption is confined to a monolayer

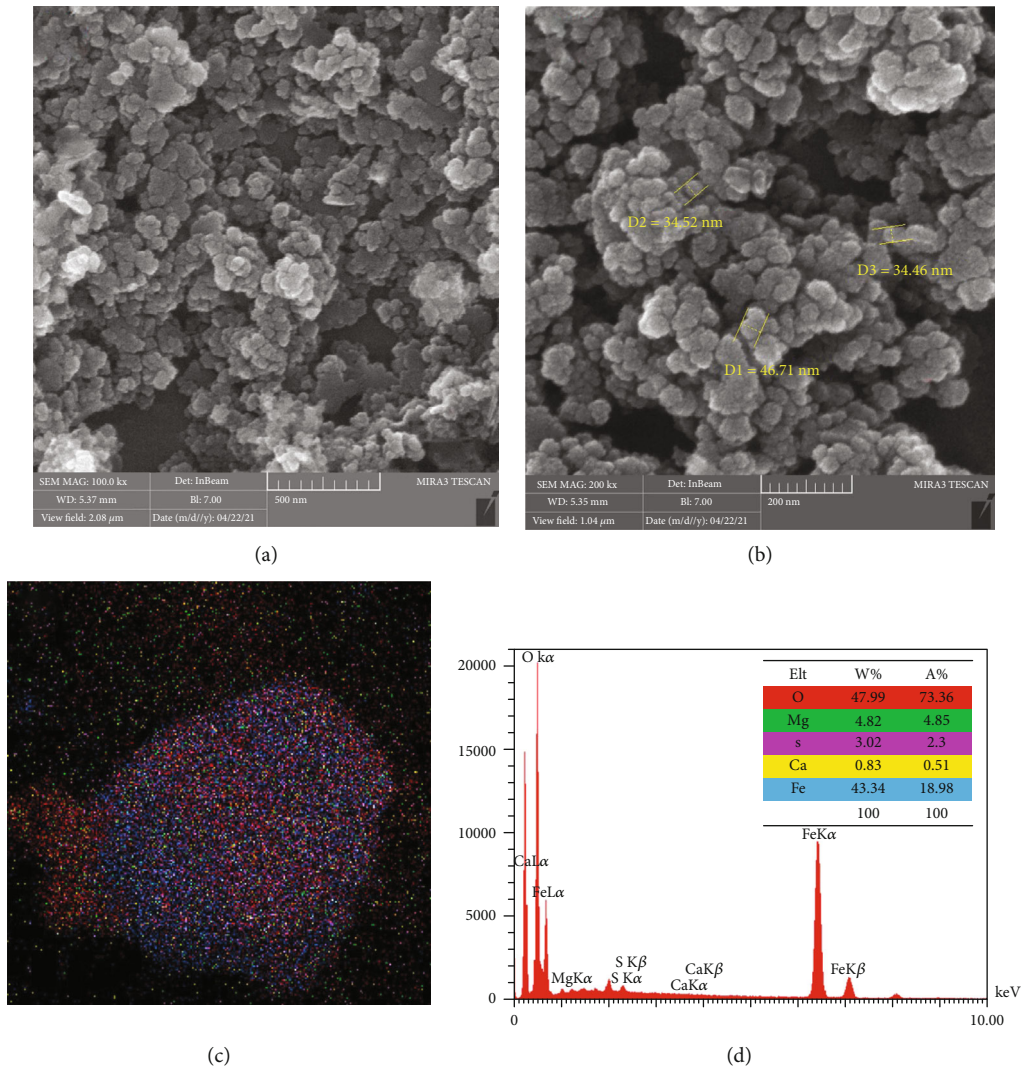

Figure 4: (a) FESEM images in 500 nm, (b) 200 nm resolutions, (c) mapping, and (d) EDX of PO–Fe_3O_4MNP magnetic nanoadsorbent.

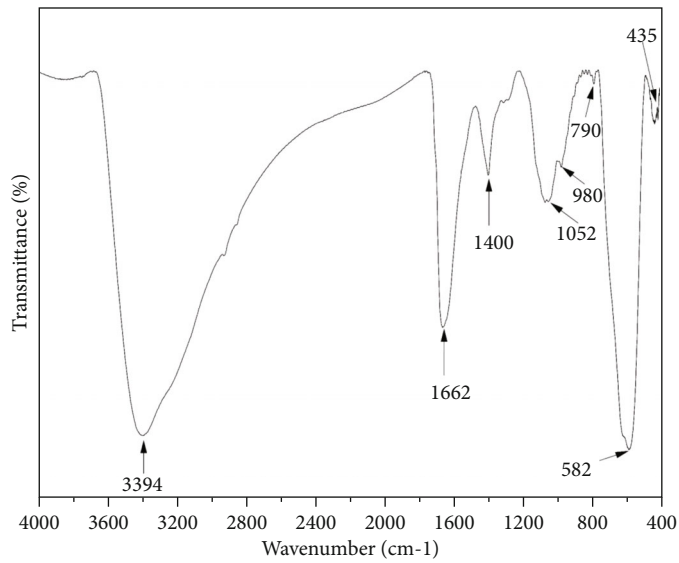

Figure 5: FTIR spectra of PO–Fe_3O_4MNPs.

[21]. The Langmuir model can be represented as

$$q_e = \frac{q_m b\, C_e}{(1 + b\, C_e)}, \tag{4}$$

where q_m (mg/g) is the Langmuir maximum adsorption capacity and b (L/mg) is the Langmuir constant [39].

The Khan isotherm model is given in

$$q_e = \frac{q_{\max} b_k C_e}{(1 + b_k C_e)^{a_k}}, \tag{5}$$

where b_k and a_k are Khan constants and $q_{\max}$ is the maximum uptake [40].

The Toth isotherm is expressed as follows:

$$q_e = \frac{q_{\max} b_k C_e}{\left[1 + (b_T C_e)^{1/n_T}\right]^{n_T}}, \tag{6}$$

where b_T and n_T are constants [41].

2.5.5. Kinetics. Adsorption kinetics describes the rate at which an adsorbate is retained or released from an aqueous environment to a solid-phase interface under various conditions [42]. The kinetic study was carried out using 0.5 g of PO–Fe_3O_4MNPs in 100 mL of single metal ion solutions with the concentration of 50 mg/L for each Pb(II) and Cd(II) at pH 6. The flasks with their contents were shaken for different adsorption times (10-70 min). The rate of sorption is analyzed by two kinetic models, namely, pseudo-first-order and pseudo-second-order.

The pseudo-first-order model explains that the rate of occupation of sorption sites is proportional to the number of unoccupied sites. The equation is represented as

$$\log (q_t - q_e) = \log q_e - \frac{k_1}{2.303}\, t, \tag{7}$$

where k_1 (min^{-1}) is the pseudo-first-order rate constant of adsorption and q_t (mg/g) and q_e (mg/g) are the amount of metal ions adsorbed at any particular time and equilibrium, respectively.

The pseudo-second-order kinetic model is based on the assumption that chemisorption is the rate-controlling step and is expressed as follows:

$$\frac{t}{q_t} = \frac{1}{k_2 q_e^2} + \frac{1}{q_e}\, t, \tag{8}$$

where k_2 (g/mg·min) is the pseudo-second-order rate constant and q_e (mg/g) and q_t (mg/g) are the amount of the metal ions adsorbed at equilibrium and at time t, respectively [21, 43].

2.5.6. Thermodynamic Parameters of Adsorption. The influence of temperature on Pb(II) and Cd(II) ion adsorption on PO–Fe_3O_4MNPs was studied at 20, 35, 45, and 55°C. About 100 mL of each solution with a concentration of 50 mg/L was mixed with 0.5 g of PO–Fe_3O_4MNPs, and then, the mixtures were maintained at a different temperature ranging from 20 to 55°C, for an hour and agitated at the speed of 200 rpm [4]. The nanoparticles were separated, and the Pb(II) and Cd(II) concentrations were measured using ICPOES.

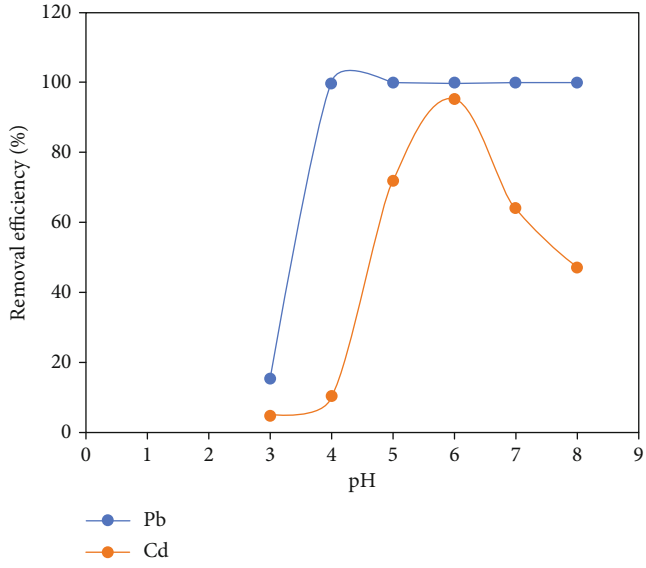

Figure 6: Effect of pH on Pb(II) and Cd(II) removal (C_o = 50 mg/L, PO–Fe_3O_4MNP dosage = 0.5 g, contact time = 60 min, temperature = 20 ± 2°C).

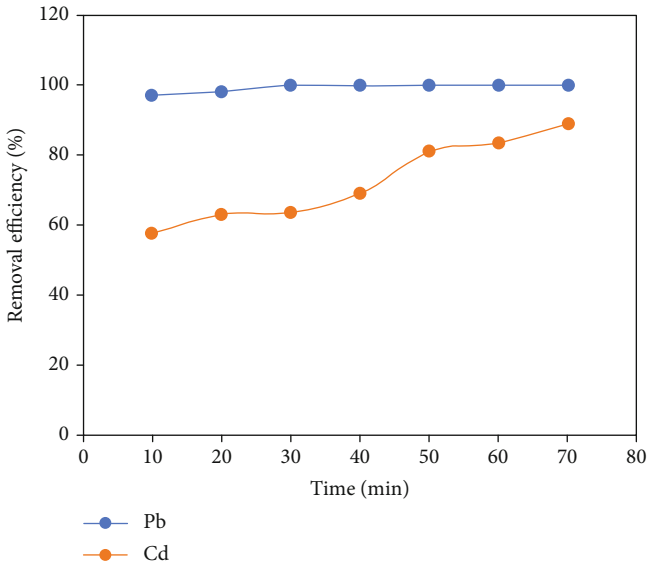

Figure 7: Effect of contact time on removal of Pb(II) and Cd(II) (C_o = 50 mg/L, PO–Fe_3O_4MNP dosage = 0.5 g, pH = 6, temperature = 20 ± 2°C).

3. Results and Discussion

3.1. PO–Fe_3O_4MNP Characterizations. The phase purity and crystalline construction of PO–Fe_3O_4MNPs are identified by

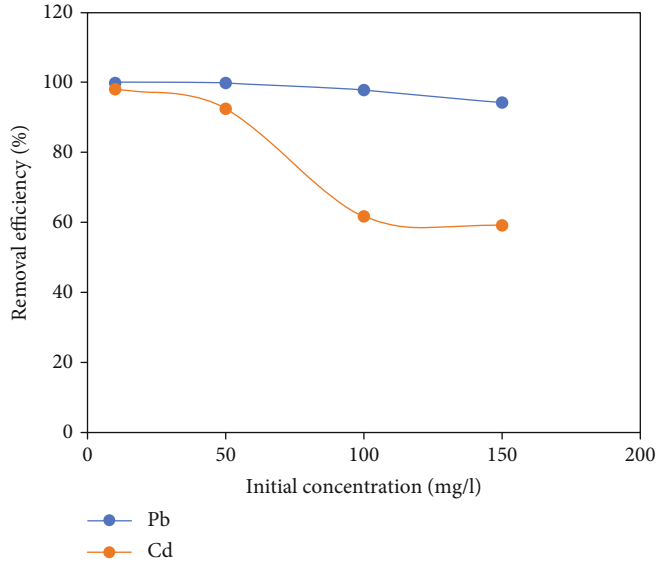

Figure 8: Effect of initial metal concentration on removal of Pb(II) and Cd(II) (PO–Fe_3O_4MNP dosage = 0.5 g, contact time = 60 min, pH = 6, temperature = 20 ± 2°C).

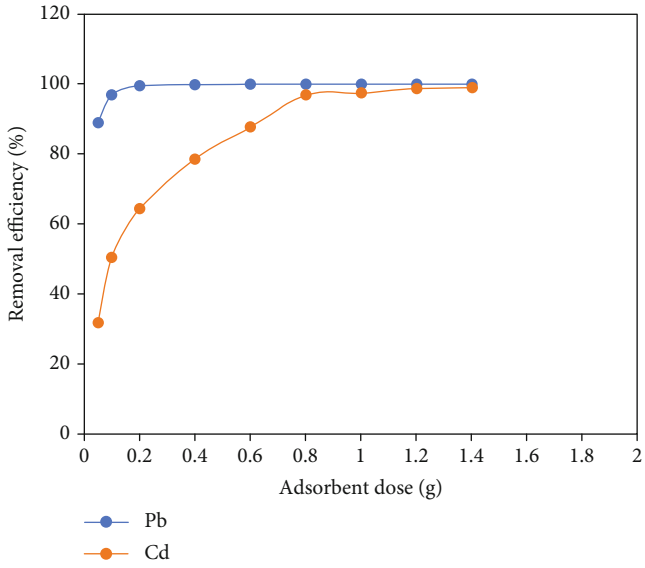

Figure 9: Effect of adsorbent dose on removal of Pb(II) and Cd(II) (C_o = 50 mg/L, contact time = 60 min, pH = 6, temperature = 20 ± 2°C).

powder XRD. Figure 2 shows the XRD pattern of dried PO–Fe_3O_4MNPs. The Bragg reflection peaks were detected at 2θ value of 30.11°, 35.47°, 43.11°, 53.48°, 57.01°, 62.61°, and 74.07°, which corresponded to the (220), (311), (400), (422), (511), (440), and (533) crystallographic planes which prove the structure of biosynthesized PO–Fe_3O_4MNPs is cubic (reference code: 96-900-5838). The XRD data is also in line with the data obtained by Rajput et al. [44] and Yew et al. [45].

Figures 3(a) and 3(b) exhibit the TEM image of the biosynthesized PO–Fe_3O_4MNPs, as well as their particle size distribution. From the TEM images, it is obvious that most of the particles were almost spherical with slight aggregation. The presence of agglomeration could be attributed to van der Waals forces that bind particles together and also shear forces that can be applied on the nanoscale [46]. The mean particle size is 26.0196 nm with a 9.05132 nm standard deviation.

The FESEM images of the PO–Fe_3O_4MNPs are shown in Figures 4(a) and 4(b). From FESEM images, it was clearly observed that the nanoparticles are bead-like, spherical in shape, with slight aggregation. Three of such nanoparticles, 34.52, 34.46, and, 46.71 nm, are mentioned in Figure 4(b). Similar spherical shapes were also reported when biosynthesis of Fe_3O_4 was conducted using leaf extract of *Mussaenda erythrophylla* [47]. X-ray elemental mapping and energy-dispersive spectroscopy (EDX) were performed to reveal the presence of elemental constituents in the PO–Fe_3O_4MNPs as shown in Figures 4(c) and 4(d). The resultant EDX spectrum of nanoparticles showed the peaks at 0.7, 6.4, and 7.2 keV for elemental iron and the peak at 0.5 keV for elemental oxygen, which confirmed the formation of the PO–Fe_3O_4MNPs. The peak at 0.3 keV revealed the existence of carbon that originated from the biomolecules of the leaf extract.

The surface functional groups and capping agents of PO–Fe_3O_4MNPs which are responsible for the reduction and stabilization were studied by FTIR spectroscopy. Figure 5 illustrates the FTIR spectrum of PO–Fe_3O_4MNPs. The peaks were observed at 582 cm^{-1} and 790 cm^{-1} due to Fe-O vibrations of Fe_3O_4 [48]. The band at 3394 cm^{-1} is attributed to the O–H group of polyphenolic compounds [49]. The band at 1662 cm^{-1} is assigned to –C=C– stretching vibration of alkenes [30]. The band at 1400 cm^{-1} belongs to C-C groups derived from aromatic rings found in the POL extract [50]. The bands between 1000 cm^{-1} and 1300 cm^{-1} were attributed to the C-O functional group in alcohols, ethers, ester,

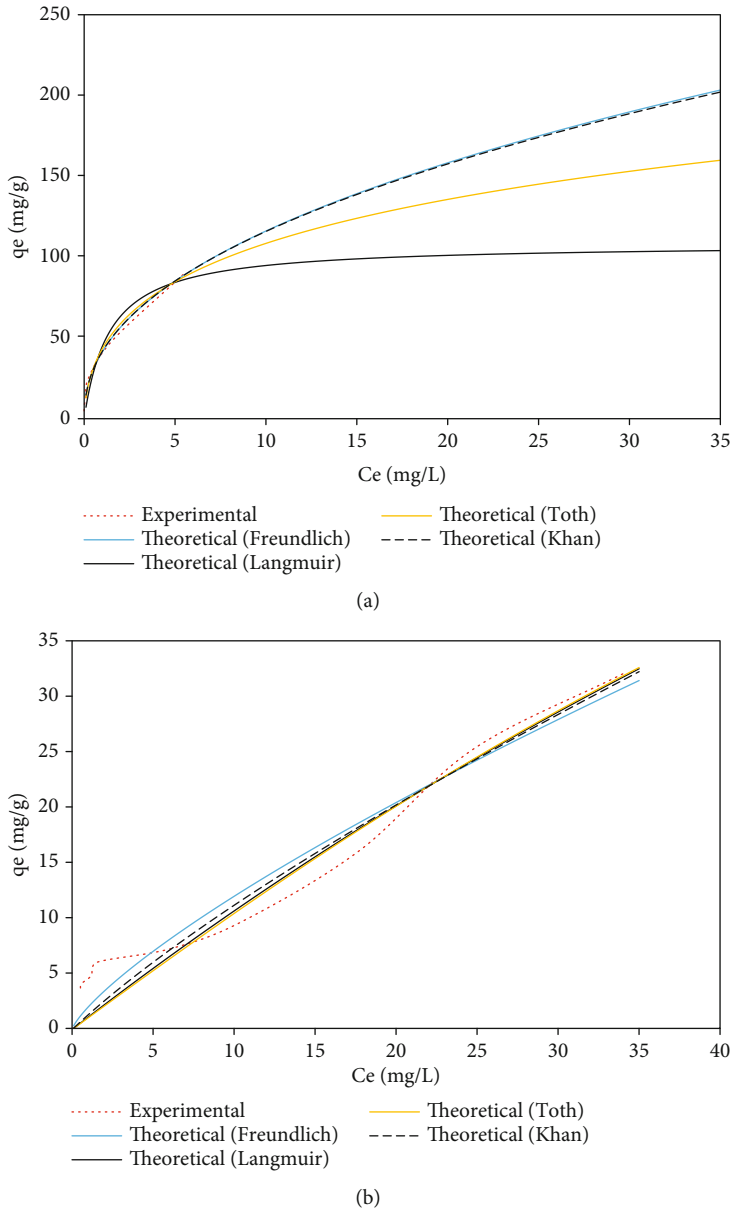

Figure 10: Comparison of isotherm models for adsorption of (a) Pb(II) and (b) Cd(II) ions onto PO–Fe_3O_4MNPs.

carboxylic acids, and amides in the extract [46]. These bands confirm the formation of PO–Fe_3O_4MNPs and showed that they were covered with polyphenols and other organic compounds which improved their stability.

3.2. Adsorption Process

3.2.1. Effect of pH. pH is the main factor that affects the efficacy of the adsorption process. In the present study, the impact of pH on Pb(II) and Cd(II) removal efficiency using biosynthesized PO–Fe_3O_4MNPs was verified at pH values ranging from 3 to 8. Pb(II) and Cd(II) adsorption was low at pH values around 3, which was attributed to electrostatic repulsion between the adsorbent and metal ions in the solution. When the concentration of hydrogen ions in the solution increases, the adsorbent sites are occupied by the hydrogen ions instead of metal ions. The protonation of active sites thus tends to decrease the metal adsorption [37]. As presented in Figure 6, the removal efficiency for Pb(II) and Cd(II) at pH 3 is found to be 15.42% and 4.8%, respectively. Maximum adsorption was recorded at higher pH 6, i.e., maximum adsorptions for Pb(II) and Cd(II) were 100% and 95.32%, respectively.

Beyond the value of pH 6, solute ions will precipitate due to the formation of insoluble metal hydroxides, which then start precipitating from the solutions at higher pH values and make the true sorption studies impossible. This should be avoided during sorption tests because it makes distinguishing between sorption and metal precipitation difficult [51]. As a result, the pH value of 6 was chosen as the optimum and

Table 1: Comparison of maximum adsorption capacity of investigated PO–Fe_3O_4MNPs for Cd(II) and Pb(II) with other adsorbents reported in the various literature.

Metal	Adsorbent	Maximum adsorption capacity (mg/g)	Reference
Cd(II)	Iron oxide nanoparticles (IONPs)	18.32	[27]
	Iron oxide nanoparticles	15.5	[37]
	Magnetite Green Fe_3O_4 nanoparticles	18.73	[52]
	DEAMTPP@Fe_3O_4MNPs	49.1	[58]
	SBA-15@Fe_3O_4@Isa	140	[59]
	c-MCM-41	32.3	[60]
	MCM-48	29.13	[61]
	PO–Fe_3O_4MNPs	177.48	This study
Pb(II)	Magnetite green Fe_3O_4 nanoparticles	0.16	[52]
	SBA-15@Fe_3O_4@Isa	110	[59]
	c-MCM-41	58.5	[60]
	MCM-48	50.39	[61]
	Iron nanocomposites (T-Fe_3O_4)	100.0	[62]
	Phytogenic magnetic nanoparticles (PMNPs)	68.41	[63]
	Fe_3O_4 nanoadsorbents	64.97	[64]
	PO–Fe_3O_4MNPs	108.2267	This study

Table 2: Parameters of Langmuir, Freundlich, Khan, and Toth isotherm models for Pb(II) and Cd(II) ions adsorption onto PO–Fe_3O_4MNPs.

Model	Parameter	Metal ions	
		Pb(II)	Cd(II)
Langmuir	q_m (mg/g)	108.2267	177.4800
	b (L/mg)	0.706296	0.006401
	R^2	0 .9439	0.92926
Freundlich	K (mg/g) (mg/L) $(1/n)$	41.48618	2.044152
	n	2.236529	1.301127
	R^2	0.97246	0.94333
Khan	q_m (mg/g)	4.025708	7.391429
	b_k (L/mg)	194.4072	0.187339
	a_k	0.556249	0.201856
	R^2	0.97245	0.93299
Toth	q_m (mg/g)	721.740333	92.02625
	b_T	2.087398	0.011593
	n_T	4.567778	0.632009
	R^2	0.96952	0.92807

used in all subsequent experiments. These results are in agreement with the results obtained by Lung et al. [52].

3.2.2. Effect of Contact Time. The influence of contact time on Pb(II) and Cd(II) removal efficiency by PO–Fe_3O_4MNPs was investigated using varying the contact time from 10 to 70 minutes. As was observed in Figure 7, the adsorption of both metal ions by PO–Fe_3O_4MNPs was increased with increasing contact time. Both metal ions have more opportunities for contact with the adsorbent surface, when time increases the availability of more active groups that are present on the surface of the adsorbent increases [22]. The removal of Pb(II) was rapid during the first 30 min. However, no significant increase in the adsorption rate was found after 30 min. The concentration of Cd(II) decreased within 50 min and remained almost constant after an hour, implying that adsorption is rapid and reaches saturation within an hour. This is a promising result because equilibrium time is critical in wastewater treatment plants that are economically viable [53].

3.2.3. Effect of Initial Metal Concentration. The effect of the initial metal concentration on the removal efficiency by 0.5 g PO–Fe_3O_4MNPs at optimal pH was investigated using solutions with varying initial metal concentrations (10, 50, 100, and 150 mg/L). Figure 8 shows that there is a lowering in adsorption of lead and cadmium ions with increasing in initial metal ion concentration in solution. The initial metal concentration plays an important role in the removal efficiency since there is a constant active binding site for a given mass of adsorbent where the fixed amount of metals can be adsorbed. Thus, increasing the metal concentration in solution against the same quantity of adsorbent decreases the adsorption capacity. These results agreed with the results obtained by Ebrahim et al. [35] and Das and Rebecca [54].

3.2.4. Effect of PO–Fe_3O_4MNP Dose. The concentration of the adsorbent is one of the most important factors influencing the efficiency of the process and adsorption capacity. In this study, the impact of the various amounts of the biosynthesized PO–Fe_3O_4MNPs varying from 0.02 to 1.4 g was studied on the removal efficiency of the Pb(II) and Cd(II) ions. Figure 9 shows that, with increasing nanoadsorbent mass, the percentage of nanoadsorbents and the adsorption percent of both Pb(II) and Cd(II) ions increase.

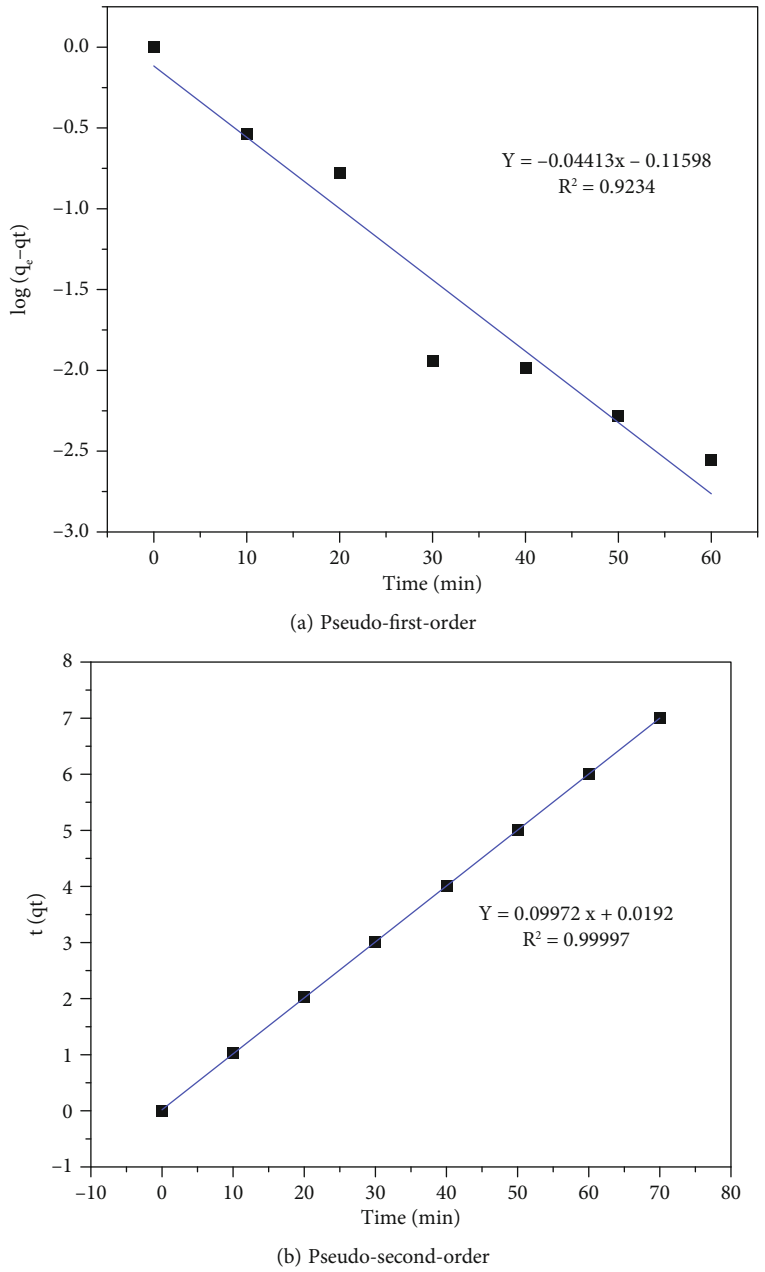

Figure 11: Adsorption kinetics for the adsorption of Pb(II) onto PO-Fe_3O_4MNPs.

This is due to the fact that at increasing dosages, there are more available sites on the surface of nanoadsorbents [55].

3.2.5. Adsorption Isotherms. The adsorption isotherms provide important information concerning adsorption capacity, the adsorption mechanism between the contaminant and the adsorbent, and the contaminant distribution between the adsorbent and the solution [4]. Adsorption isotherms were determined by fitting the experimental data obtained at equilibrium time, with the isotherm models including Freundlich, Langmuir, Toth, and Khan. The Langmuir adsorption isotherm is based on monolayer adsorption on the surface and assumes a homogenous sorbent surface [39]. The Toth isotherm is an empirical modification of the Langmuir equation that is aimed at reducing the error between experimental and predicted equilibrium data. This method is especially useful for explaining systems with heterogeneous adsorption [40]. The Freundlich isotherm can be applied to adsorption processes on heterogonous surfaces; it gives the concept of multilayer adsorption and the exponential distribution of active sites on the surface of the sorbent [56]. Finally, the Khan isotherm represents both the Langmuir and Freundlich models, suggested for adsorbate adsorption from pure solutions [40].

Figures 10(a) and 10(b) show the comparison of Freundlich, Langmuir, Khan, and Toth models for lead and cadmium ions, respectively. The Freundlich model fits the experimental data better than the Langmuir, Khan,

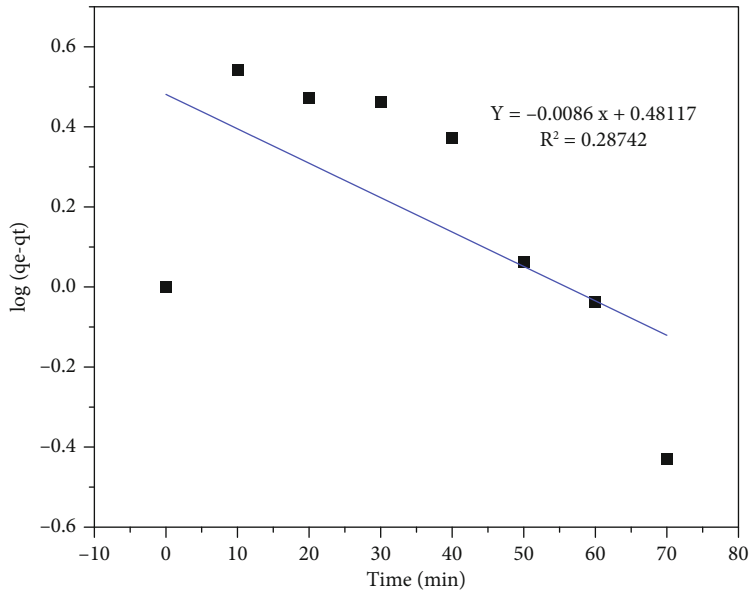

(a) Pseudo-first-order

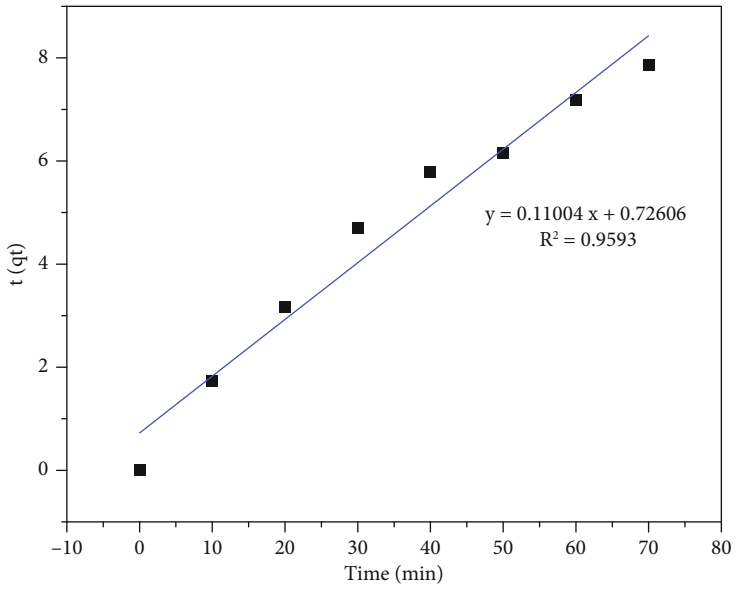

(b) Pseudo-second-order

Figure 12: Adsorption kinetics for the adsorption of Cd(II) onto PO-Fe_3O_4MNPs.

Table 3: Kinetic parameters for Pb(II) and Cd(II) ion biosorption onto PO–Fe_3O_4MNPs.

Metals	Pseudo-first-order			Pseudo-second-order		
	q_e (mg/g)	K_1 (min^{-1})	R^2	q_e (mg/g)	K_2 (g/mg min)	R^2
Pb(II)	0.7656	0.1016	0.9234	10.0280	0.5179	0.9999
Cd(II)	3.0280	0.0198	0.2874	9.0876	0.0166	0.9593

and Toth models based on the correlation coefficients, which denotes multilayer adsorption of Pb(II) and Cd(II). It was noticed that values of n for cadmium and lead were 1.301 and 2.236, respectively, indicating favorable adsorption between PO–Fe_3O_4MNPs and the metal ions. Table 1 illustrates the adsorption capacity of PO–Fe_3O_4MNPs compared to other adsorbents that have been reported in various literature. The adsorption capacity was 177.48 mg/g for cadmium and 108.2267 mg/g for lead (Table 2). This indicates that the adsorption capacity of

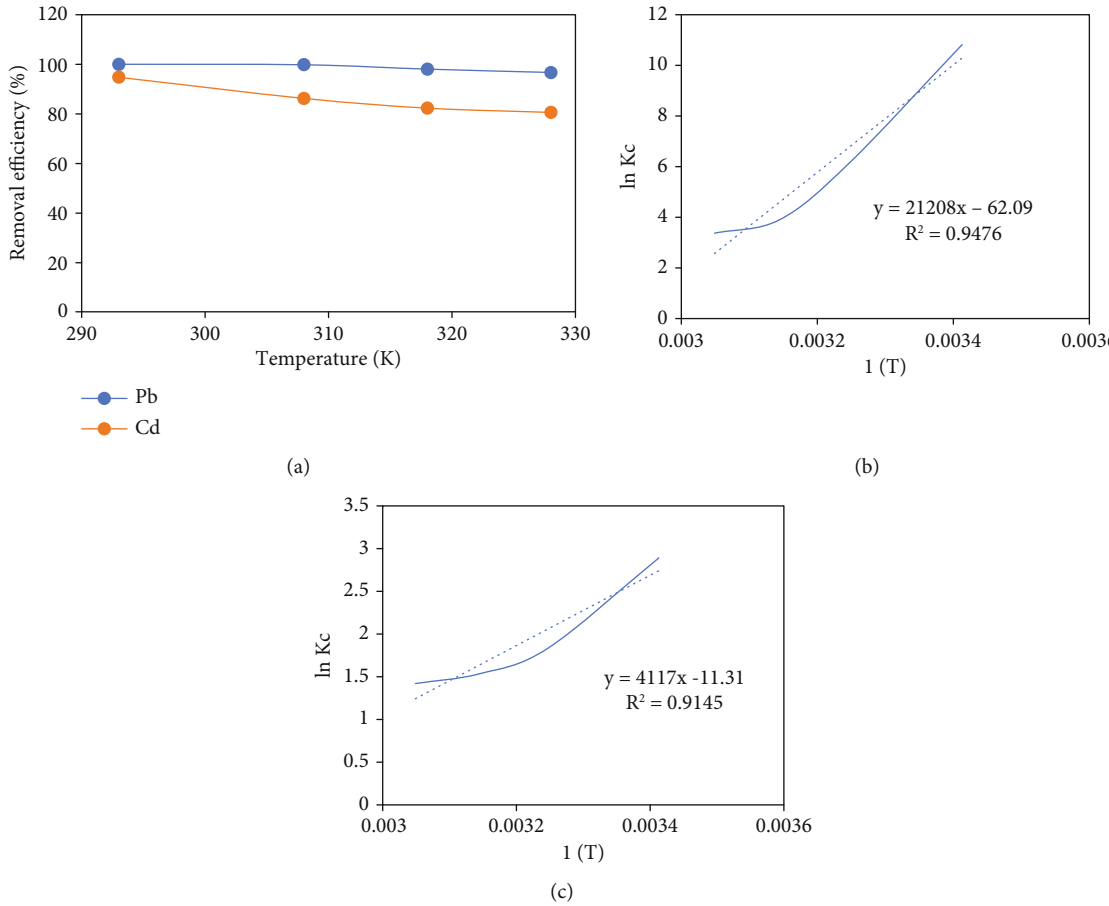

Figure 13: (a) Effect of temperature on the Pb(II) and Cd(II) ion removal; (b) thermodynamic plot for Pb(II); (c) thermodynamic plot for Cd(II) adsorption.

Table 4: Thermodynamic parameters for Pb(II) and Cd(II) adsorption onto PO–Fe_3O_4MNPs.

Metal	Temperature (K)	ΔG° (kJ/mol)	ΔH° (kJ/mol)	ΔS° (kJ/mol/K)	R^2
Pb(II)	293	-26.35695282	-176.323312	-0.51621626	0.9476
	308	-15.71120935			
	318	-10.32196239			
	328	-9.193894743			
Cd(II)	293	-7.042494622	-34.228738	-0.09403134	0.9145
	308	-4.691228444			
	318	-4.05764763			
	328	-3.873400017			

PO–Fe_3O_4MNPs is higher than that of most of the adsorbents listed in Table 1.

As illustrated in Figure 9, advanced adsorption removal for the lead was achieved at a low dose of PO–Fe_3O_4MNPs and it has a more rapid affinity towards the nanoparticles as compared to cadmium ions, which reveals the presence of various electrical attractions between cation lead metal and negative adsorption functional sites. Additionally, the lead ion possesses the smallest hydration radius; this agrees with the conception that ions with a small hydration radius are desirably selected and gathered at the interface [51, 57].

3.2.6. Kinetics. The kinetics of Cd(II) and Pb(II) adsorption on PO-Fe_3O_4MNPs were studied using pseudo-first-order and pseudo-second-order kinetic models, as demonstrated in Figures 11 and 12. The kinetic parameters and correlation coefficients R^2 are documented in Table 3. Cd(II) and Pb(II) adsorption data were well fitted to pseudo-second-order equation ($R^2 > 0.99$ Pb(II); 0.95 Cd(II)). Thus, chemisorption is

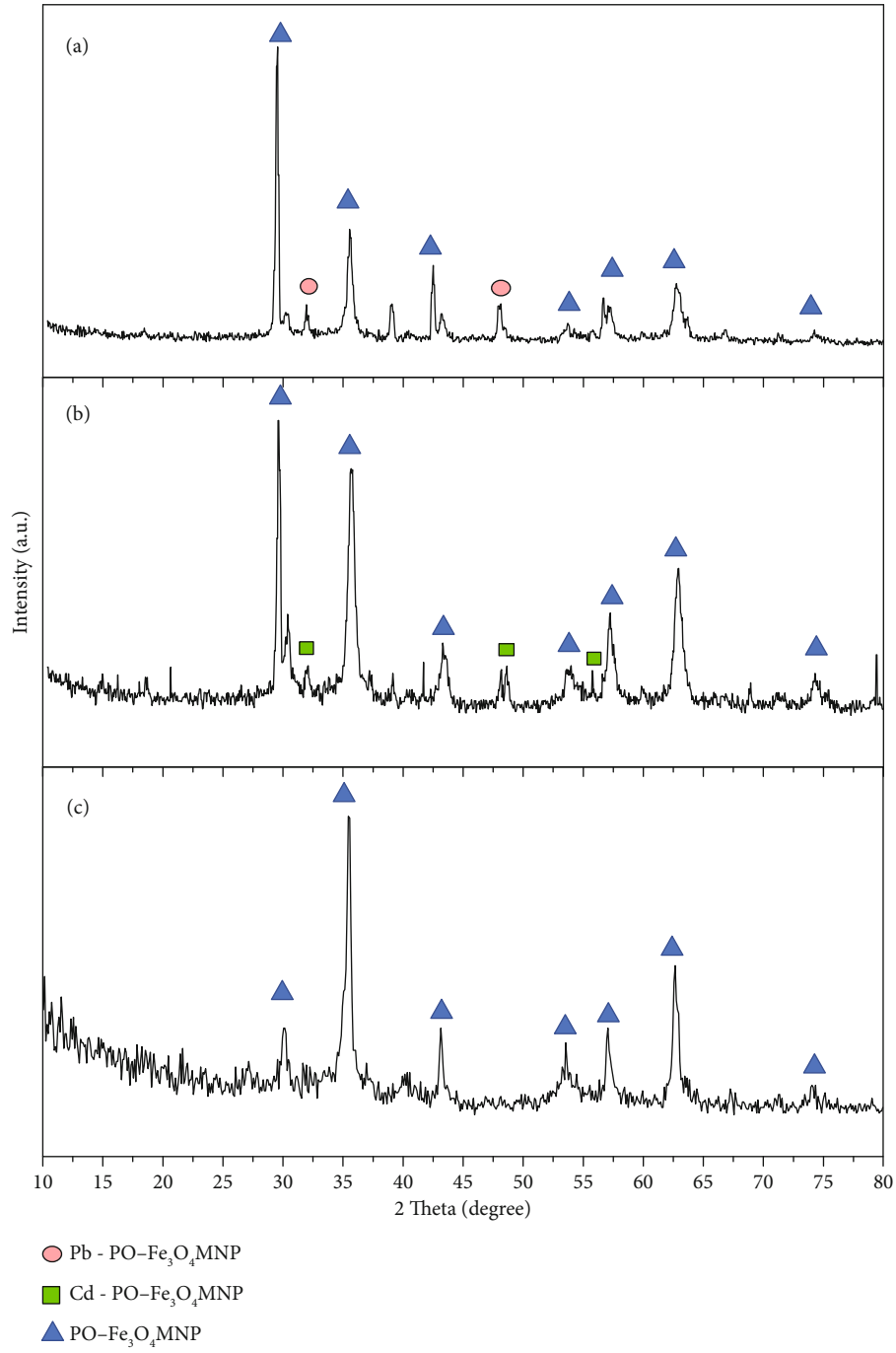

Figure 14: XRD spectra of (a) lead-loaded PO–Fe_3O_4MNPs, (b) cadmium-loaded PO–Fe_3O_4MNPs, and (c) PO–Fe_3O_4MNPs.

the rate-determining step for Cd(II) and Pb(II) adsorption on PO-Fe_3O_4MNPs through sharing or exchanging of electrons, between the sorbent and the sorbate [26, 65].

3.2.7. Thermodynamic Analysis. Temperature is another important factor that influences the remediation efficiency of the adsorption process. Figure 13(a) shows the variation of percentage removal efficiency with temperature. It is obvious from the results that changing the temperature from 20 to 35°C has no significant effect on the sorption of adsorbents so the adsorption experiments can be carried out at room temperature without any adjustment. Similar results were reported by Rasheed and Ebrahim [51]. However, removal efficiency decreases beyond 35°C due to a reduction in the number of active surface sites available for adsorption on the adsorbent [66]. Furthermore, at high temperatures, the attractive forces between the adsorbent and adsorbate become weaker, and therefore, sorption decreases [22]. In the temperature range of 20–55°C, the thermodynamic aspect of the adsorption of Pb(II) and Cd(II) ions on PO–Fe_3O_4MNPs was determined to show if the process was endothermic or exothermic. Thermodynamic parameters

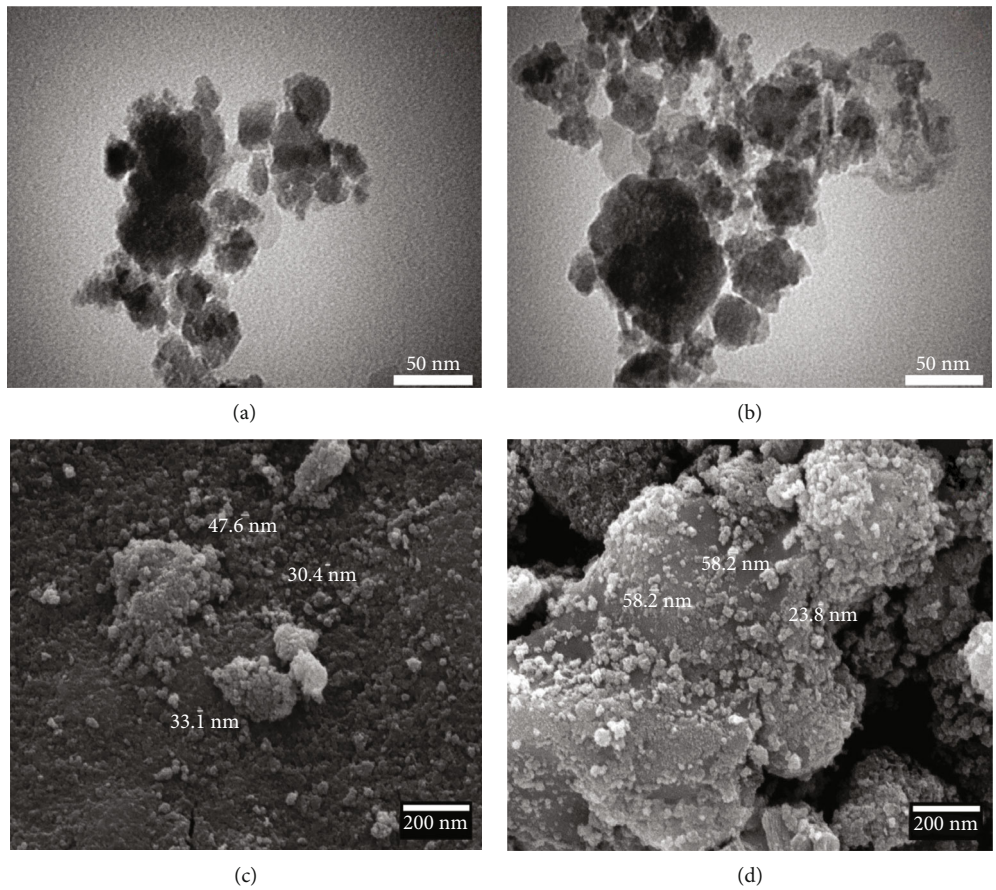

Figure 15: TEM images of (a) cadmium-loaded PO–Fe_3O_4MNPs and (b) lead-loaded PO–Fe_3O_4MNPs; FESEM images of (c) cadmium-loaded PO–Fe_3O_4MNPs and (d) lead-loaded PO–Fe_3O_4MNPs.

including Gibb's free energy (ΔG°), enthalpy (ΔH°), and entropy (ΔS°) are obtained using the following equation:

$$\Delta G^\circ = -RT \ln K_c \quad K_c = \frac{C_{ad}}{C_e}, \tag{9}$$

$$\Delta G^\circ = \Delta H^\circ - T\Delta S^\circ. \tag{10}$$

In these equations, R is the ideal gas constant, T is the absolute temperature (K), K_c is the equilibrium constant, C_{ad} is the amount of Pb(II) and Cd(II) adsorbed on PO–Fe_3O_4MNPs per liter of the solution (mg/L), and C_e is the equilibrium concentration of Pb(II) and Cd(II) in the solution (mg/L). The enthalpy and entropy change values *were* calculated from the slope and intercept of the plot of $\ln K_c$ versus $1/T$ as shown in Figures 13(b) and 13(c). The calculated ΔG°, ΔH°, and ΔS° are arranged in Table 4. The negative values of ΔG° illustrate the spontaneity and feasibility of the adsorption reaction at a given temperature, and the increasing value of ΔG° with an increased temperature indicates a decrease in the degree of feasibility for Pb(II) and Cd(II) adsorption. To be thermodynamically acceptable, ΔG° must always be negative [21]. The negative values of ΔH°, -176.323312 for Pb(II) ions and -34.228738 kJ/mol for Cd(II) ions, show that the adsorption is exothermic. Moreover, the ΔS° values for Pb(II) and Cd(II) ions at the mentioned temperatures are obtained as -0.51621626 and -0.09403134 kJ/mol/K, respectively. These negative values indicate reducing the irregularity or randomness in the adsorbate–adsorbent interface during Pb(II) and Cd(II) adsorption.

3.2.8. Characterizations of Pb(II)- and Cd(II)-Loaded PO–Fe_3O_4MNPs. Pb(II) and Cd(II) uptake onto PO–Fe_3O_4MNPs was confirmed by using XRD, TEM, FESEM, EDX, and elemental mapping of Pb(II)- and Cd(II)-loaded PO–Fe_3O_4MNPs. About 0.5 g of PO–Fe_3O_4MNPs was agitated within 50 mg/L of Pb(II) and Cd(II) solution at optimal conditions (temperature: $20 \pm 2^\circ$C, pH: 6, agitation speed: 200 rpm; equilibrium time: 60 min). The suspension was filtered using Whatman filter paper (no. 1), and the residue was dried in an oven at 50°C overnight.

The XRD patterns of Pb(II)- and Cd(II)-loaded PO–Fe_3O_4MNPs are shown in Figure 14. It was noted that after adsorption of Cd(II) by PO–Fe_3O_4MNPs, three peaks, which are centered at 32, 48, and 55°, were observed, attributed to the presence of the Cd(II) ions. In case of Pb(II) adsorption, two peaks were observed, which are centered at 31 and 48°. In addition, XRD spectra showed that there were no changes in the peaks of PO–Fe_3O_4MNPs; this confirms the adsorption of Cd(II) and Pb(II) ions on the surface of PO–Fe_3O_4MNPs.

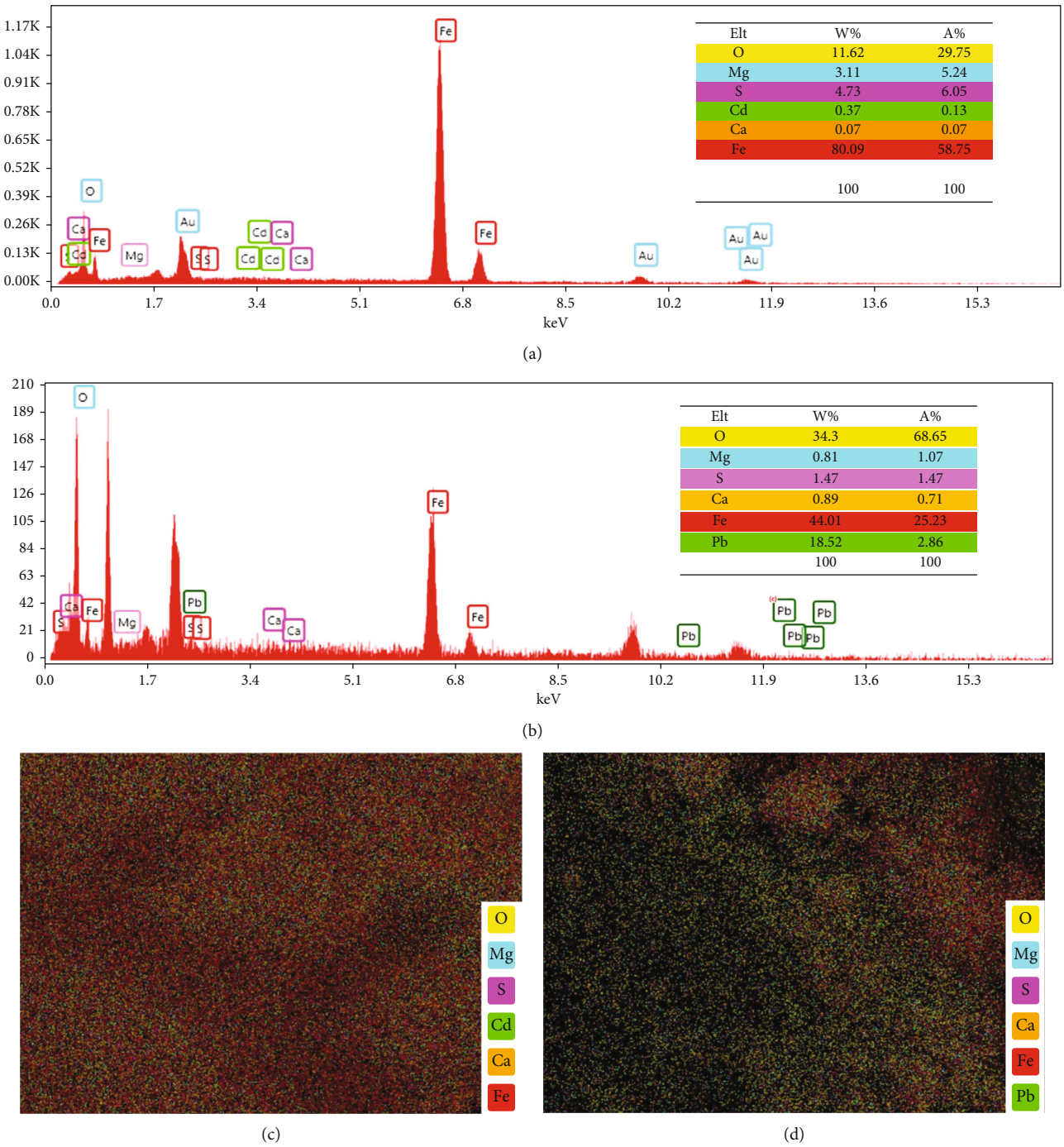

Figure 16: EDX spectra of (a) cadmium-loaded PO–Fe_3O_4MNPs and (b) lead-loaded PO–Fe_3O_4MNPs; elemental mapping images of (c) cadmium-loaded PO–Fe_3O_4MNPs and (d) lead-loaded PO–Fe_3O_4MNPs.

The TEM images of PO–Fe_3O_4MNPs after Cd(II) and Pb(II) adsorptions are shown in Figures 15(a) and 15(b). Many black particles were observed which may be attributed to the existence of higher concentrations of surface-bound metal ions which result in small accumulation of the particles after adsorption and also indicates the magnetic property of PO–Fe_3O_4MNPs. Similar results were reported by Lin et al. [27].

FESEM was used to show the morphology and topographic features of Pb(II)- and Cd(II)-loaded PO–Fe_3O_4MNPs. FESEM images revealed some aggregations and a slight increase in the dimensions of PO–Fe_3O_4MNPs as shown in Figures 15(c) and 15(d). However, the morphology of individual nanoparticles barely changed, indicating that the removal of Pb(II) and Cd(II) ions was performed by the adsorption process.

The EDX analysis of PO–Fe_3O_4MNPs after adsorption of Cd(II) and Pb(II) is presented graphically in Figures 16(a) and 16(b). The EDX patterns show the existence of magnesium, oxygen, sulfur, iron, calcium, and cadmium on the surface of cadmium-loaded PO–Fe_3O_4MNPs, and the distribution of oxygen, magnesium, calcium, sulfur, iron, and lead on the surface of lead-loaded PO–Fe_3O_4MNPs clearly confirms successful adsorption of Pb(II) and Cd(II) on PO–Fe_3O_4MNP surfaces. The results show a good agreement with those obtained by Bagbi et al. [67]. The elemental mapping also confirmed the adsorption of Pb(II) (in green) and Cd(II) (in green) as shown in Figures 16(c) and 16(d). It is clear that Pb(II) and Cd(II) ions are uniformly distributed on the surface of PO–Fe_3O_4MNPs.

4. Conclusion

In this study, *Portulaca oleracea* leaf extract was successfully used as a reductant in PO–Fe_3O_4MNP synthesizing process. The biosynthesized PO–Fe_3O_4MNPs were characterized and used as adsorbents for the removal of Pb(II) and Cd(II) metal ions from the aqueous solution in batch adsorption system. The batch experiments showed that the removal efficiency of Pb(II) and Cd(II) by PO–Fe_3O_4MNPs increased with increasing pH (up to 6), contact time, and PO–Fe_3O_4MNP dosage. On the other hand, an increase in metal concentration and temperature resulted in reduced Pb(II) and Cd(II) removal efficiency of PO–Fe_3O_4MNPs. Isotherm studies revealed that the Freundlich model can properly predict adsorption equilibrium data, which indicates multilayer adsorption. The kinetic studies suggested pseudo-second-order reactions for the adsorption, while thermodynamic studies demonstrated the adsorption as exothermic and spontaneous. This study shows that PO–Fe_3O_4MNPs can be considered fast, efficient, and biocompatible nanoadsorbent which have promising applications in environmental remediation processes and nanobiotechnology in the future.

Data Availability

The data sets used and analyzed during the current study are available within the article only.

Conflicts of Interest

The authors have no conflict of interest.

Acknowledgments

The authors acknowledge the kind help of Professor Dr. Khalid Mohammed Omer for his support and guidance in the synthesis of the nanoparticles and Dr. Bruska Azhdar and Dr. Farouk Abdullah Rasheed for their useful assistance in the calculations of surface area of the magnetite nanoparticles and isothermal parameters.

References

[1] A. Boretti and L. Rosa, "Reassessing the projections of the World Water Development Report," *Water*, vol. 2, no. 1, 2019.

[2] J. Ahmed, A. Thakur, and A. Goyal, "CHAPTER 1 industrial wastewater and its toxic effects," in *Biological Treatment of Industrial Wastewater*, pp. 1–14, The Royal Society of Chemistry, 2022.

[3] R. Gusain, N. Kumar, E. Fosso-Kankeu, and S. S. Ray, "Efficient removal of Pb(II) and Cd(II) from industrial mine water by a hierarchical MoS2/SH-MWCNT nanocomposite," *ACS Omega*, vol. 4, no. 9, pp. 13922–13935, 2019.

[4] R. Pelalak, Z. Heidari, S. M. Khatami, T. A. Kurniawan, A. Marjani, and S. Shirazian, "Oak wood_ ash/GO/Fe_3O_4 adsorption efficiencies for cadmium and lead removal from aqueous solution: kinetics, equilibrium and thermodynamic evaluation," *Arabian Journal of Chemistry*, vol. 14, no. 3, article 102991, 2021.

[5] Y. A. Abd Al-Khodor and T. M. Albayati, "Employing sodium hydroxide in desulfurization of the actual heavy crude oil: theoretical optimization and experimental evaluation," *Process Safety and Environmental Protection*, vol. 136, pp. 334–342, 2020.

[6] P. J. Landrigan, J. J. Stegeman, L. E. Fleming et al., "Human health and ocean pollution," *Annals of Global Health*, vol. 86, no. 1, pp. 151–151, 2020.

[7] S. M. Alardhi, J. M. Alrubaye, and T. M. Albayati, "Removal of methyl green dye from simulated waste water using hollow fiber ultrafiltration membrane," *IOP Conference Series: Materials Science and Engineering*, vol. 928, no. 5, article 052020, 2020.

[8] S. Mahanty, S. Chatterjee, S. Ghosh et al., "Synergistic approach towards the sustainable management of heavy metals in wastewater using mycosynthesized iron oxide nanoparticles: biofabrication, adsorptive dynamics and chemometric modeling study," *Journal of Water Process Engineering*, vol. 37, article 101426, 2020.

[9] S. Mitra, A. J. Chakraborty, A. M. Tareq et al., "Impact of heavy metals on the environment and human health: novel therapeutic insights to counter the toxicity," *Journal of King Saud University - Science*, vol. 34, no. 3, article 101865, 2022.

[10] H. Ali, E. Khan, and I. Ilahi, "Environmental chemistry and ecotoxicology of hazardous heavy metals: environmental persistence, toxicity, and bioaccumulation," *Journal of Chemistry*, vol. 2019, 14 pages, 2019.

[11] M. M. Uddin, M. C. M. Zakeel, J. S. Zavahir, F. M. M. T. Marikar, and I. Jahan, "Heavy metal accumulation in rice and aquatic plants used as human food: a general review," *Toxics*, vol. 9, no. 12, p. 360, 2021.

[12] A.-M. Yang, K. Lo, T. Z. Zheng et al., "Environmental heavy metals and cardiovascular diseases: status and future direction," *Chronic Diseases and Translational Medicine*, vol. 6, no. 4, pp. 251–259, 2020.

[13] O. Stoian, C. I. Covaliu, G. Paraschiv et al., "Magnetite oxide nanomaterial used for lead ions removal from industrial wastewater," *Materials (Basel, Switzerland)*, vol. 14, no. 11, p. 2831, 2021.

[14] S. Wan, J. Wu, S. Zhou, R. Wang, B. Gao, and F. He, "Enhanced lead and cadmium removal using biochar-supported hydrated manganese oxide (HMO) nanoparticles: behavior and mechanism," *Science of the Total Environment*, vol. 616-617, pp. 1298–1306, 2018.

[15] R. Vidu, E. Matei, A. M. Predescu et al., "Removal of heavy metals from wastewaters: a challenge from current treatment methods to nanotechnology applications," *Toxics*, vol. 8, no. 4, p. 101, 2020.

[16] T. A. Saleh, M. Mustaqeem, and M. Khaled, "Water treatment technologies in removing heavy metal ions from wastewater: a review," *Environmental Nanotechnology, Monitoring & Management*, vol. 17, article 100617, 2022.

[17] K. R. Kalash and T. M. Albayati, "Remediation of oil refinery wastewater implementing functionalized mesoporous materials MCM-41 in batch and continuous adsorption process," *DESALINATION WATER TREATMENT*, vol. 220, pp. 130–141, 2021.

[18] S. T. Kadhum, G. Y. Alkindi, and T. M. Albayati, "Remediation of phenolic wastewater implementing nano zerovalent iron as a granular third electrode in an electrochemical reactor," *International journal of Environmental Science and Technology*, vol. 19, no. 3, pp. 1383–1392, 2022.

[19] W. Peng, H. Li, Y. Liu, and S. Song, "A review on heavy metal ions adsorption from water by graphene oxide and its composites," *Journal of Molecular Liquids*, vol. 230, pp. 496–504, 2017.

[20] A. El-Denglawey, M. F. Mubarak, and H. Selim, "Tertiary nanocomposites of metakaolinite/Fe_3O_4/SBA-15 nanocomposite for the heavy metal adsorption: isotherm and kinetic study," *Arabian Journal for Science and Engineering*, vol. 47, no. 1, pp. 455–476, 2022.

[21] S. Alardhi, J. Alrubaye, and T. Albayati, "Adsorption of methyl green dye onto MCM-41: equilibrium, kinetics and thermodynamic studies," *Desalination and Water Treatment*, vol. 179, pp. 323–331, 2020.

[22] R. Singh and R. Bhateria, "Experimental and modeling process optimization of lead adsorption on magnetite nanoparticles via isothermal, kinetics, and thermodynamic studies," *ACS Omega*, vol. 5, no. 19, pp. 10826–10837, 2020.

[23] N. Zhu, H. Ji, P. Yu et al., "Surface modification of magnetic iron oxide nanoparticles," *Nanomaterials (Basel)*, vol. 8, no. 10, p. 810, 2018.

[24] V. Kamath, P. Chandra, and G. P. Jeppu, "Comparative study of using five different leaf extracts in the green synthesis of iron oxide nanoparticles for removal of arsenic from water," *International Journal of Phytoremediation*, vol. 22, no. 12, pp. 1278–1294, 2020.

[25] Y. C. López and M. Antuch, "Morphology control in the plant-mediated synthesis of magnetite nanoparticles," *Current Opinion in Green and Sustainable Chemistry*, vol. 24, pp. 32–37, 2020.

[26] N. Kataria and V. K. Garg, "Green synthesis of Fe_3O_4 nanoparticles loaded sawdust carbon for cadmium (II) removal from water: regeneration and mechanism," *Chemosphere*, vol. 208, pp. 818–828, 2018.

[27] J. Lin, B. Su, M. Sun, B. Chen, and Z. Chen, "Biosynthesized iron oxide nanoparticles used for optimized removal of cadmium with response surface methodology," *Science of the Total Environment*, vol. 627, pp. 314–321, 2018.

[28] Y. Vitta, M. Figueroa, M. Calderon, and C. Ciangherotti, "Synthesis of iron nanoparticles from aqueous extract of _Eucalyptus robusta_ Sm and evaluation of antioxidant and antimicrobial activity," *Materials Science for Energy Technologies*, vol. 3, pp. 97–103, 2020.

[29] M. M. Kgatitsoe, S. Ncube, H. Tutu, I. A. Nyambe, and L. Chimuka, "Synthesis and characterization of a magnetic nanosorbent modified with _Moringa oleifera_ leaf extracts for removal of nitroaromatic explosive compounds in water samples," *Journal of Environmental Chemical Engineering*, vol. 7, no. 3, article 103128, 2019.

[30] K. Sirdeshpande, A. Sridhar, K. M. Cholkar, and R. Selvaraj, "Structural characterization of mesoporous magnetite nanoparticles synthesized using the leaf extract of Calliandra haematocephala and their photocatalytic degradation of malachite green dye," *Applied Nano*, vol. 8, no. 4, pp. 675–683, 2018.

[31] G. D. Saratale, R. G. Saratale, S. K. Cho et al., "Investigation of photocatalytic degradation of reactive textile dyes by _Portulaca oleracea_ -functionalized silver nanocomposites and exploration of their antibacterial and antidiabetic potentials," *Journal of Alloys and Compounds*, vol. 833, article 155083, 2020.

[32] M. Jamzad, M. Kamari Bidkorpeh, and F. Naderi, "Potential evaluation of the aqueous extract of Portulaca oleracea L. in the synthesis of iron oxide nanoparticles," *Eco-phytochemical Journal of Medicinal Plants*, vol. 7, no. 2, pp. 117–128, 2019.

[33] R. Selvaraj, S. Pai, G. Murugesan et al., "Green synthesis of magnetic α–Fe2O3 nanospheres using Bridelia retusa leaf extract for Fenton-like degradation of crystal violet dye," *Applied Nanoscience*, vol. 11, no. 8, pp. 2227–2234, 2021.

[34] F. I. El-Dib, D. E. Mohamed, O. A. A. El-Shamy, and M. R. Mishrif, "Study the adsorption properties of magnetite nanoparticles in the presence of different synthesized surfactants for heavy metal ions removal," *Egyptian Journal of Petroleum*, vol. 29, no. 1, pp. 1–7, 2020.

[35] S. Ebrahim, A. Sulaymon, and H. Alhares, "Competitive removal of Cu 2+ , Cd 2+ , Zn 2+ , and Ni 2+ ions onto iron oxide nanoparticles from wastewater," *Desalination and Water Treatment*, vol. 57, 2015.

[36] E. H. Khader, T. J. Mohammed, and T. M. Albayati, "Comparative performance between rice husk and granular activated carbon for the removal of azo tartrazine dye from aqueous solution," *Desalination and Water Treatment*, vol. 229, pp. 372–383, 2021.

[37] M. H. Ehrampoush, M. Miria, M. H. Salmani, and A. H. Mahvi, "Cadmium removal from aqueous solution by green synthesis iron oxide nanoparticles with tangerine peel extract," *Journal of Environmental Health Science and Engineering*, vol. 13, no. 1, p. 84, 2015.

[38] J. López-Luna, L. E. Ramírez-Montes, S. Martinez-Vargas et al., "Linear and nonlinear kinetic and isotherm adsorption models for arsenic removal by manganese ferrite nanoparticles," *SN Applied Sciences*, vol. 1, no. 8, 2019.

[39] A. Andelescu, M. A. Nistor, S. G. Muntean, and M. E. Rădulescu-Grad, "Adsorption studies on copper, cadmium, and zinc ion removal from aqueous solution using magnetite/carbon nanocomposites," *Separation Science and Technology*, vol. 53, no. 15, pp. 2352–2364, 2018.

[40] M. A. Al-Ghouti and D. A. Da'ana, "Guidelines for the use and interpretation of adsorption isotherm models: a review," *Journal of Hazardous Materials*, vol. 393, article 122383, 2020.

[41] K. Kiełbasa, A. Kamińska, O. Niedoba, and B. Michalkiewicz, "CO_2 adsorption on activated carbons prepared from molasses: a comparison of two and three parametric models," *Materials (Basel, Switzerland)*, vol. 14, no. 23, 2021.

[42] M. Manjuladevi, R. Anitha, and S. Manonmani, "Kinetic study on adsorption of Cr(VI), Ni(II), Cd(II) and Pb(II) ions from aqueous solutions using activated carbon prepared from Cucumis melo peel," *Applied Water Science*, vol. 8, no. 1, 2018.

[43] Y. Bagbi, A. Sarswat, D. Mohan, A. Pandey, and P. R. Solanki, "Lead and chromium adsorption from water using L-cysteine

functionalized magnetite (Fe_3O_4) nanoparticles," *Scientific Reports*, vol. 7, no. 1, p. 7672, 2017.

[44] S. Rajput, C. U. Pittman, and D. Mohan, "Magnetic magnetite (Fe_3O_4) nanoparticle synthesis and applications for lead (Pb^{2+}) and chromium (Cr^{6+}) removal from water," *Journal of Colloid and Interface Science*, vol. 468, pp. 334–346, 2016.

[45] Y. P. Yew, K. Shameli, M. Miyake et al., "Green synthesis of magnetite (Fe_3O_4) nanoparticles using seaweed (Kappaphycus alvarezii) extract," *Nanoscale Research Letters*, vol. 11, no. 1, p. 276, 2016.

[46] M. Yusefi, K. Shameli, O. Su Yee et al., "Green synthesis of Fe_3O_4 nanoparticles stabilized by a Garcinia mangostana fruit peel extract for hyperthermia and anticancer activities," *International Journal of Nanomedicine*, vol. Volume 16, pp. 2515–2532, 2021.

[47] R. Vinayagam, C. Zhou, S. Pai et al., "Structural characterization of green synthesized magnetic mesoporous Fe_3O_4," *Materials Chemistry and Physics*, vol. 262, article 124323, 2021.

[48] M. J. K. Ahmed, M. Ahmaruzzaman, and M. H. Bordoloi, "Novel Averrhoa carambola extract stabilized magnetite nanoparticles: a green synthesis route for the removal of chlorazol black E from wastewater," *RSC Advances*, vol. 5, no. 91, pp. 74645–74655, 2015.

[49] P. K. Dhar, P. Saha, M. K. Hasan, M. K. Amin, and M. R. Haque, "Green synthesis of magnetite nanoparticles using _Lathyrus sativus_ peel extract and evaluation of their catalytic activity," *Cleaner Engineering and Technology*, vol. 3, article 100117, 2021.

[50] Z. Izadiyan, K. Shameli, M. Miyake et al., "Cytotoxicity assay of plant-mediated synthesized iron oxide nanoparticles using _Juglans regia_ green husk extract," *Arabian Journal of Chemistry*, vol. 13, no. 1, pp. 2011–2023, 2020.

[51] F. Rasheed and S. Ebrahim, "Comparison between dead anaerobic biomass and synthesized Fe3O4 nanoparticles for the removal of Pb(II), Ni(II) and Cd(II)," *Desalination and Water Treatment*, vol. 173, pp. 351–366, 2020.

[52] I. Lung, M. Stan, O. Opris, M. L. Soran, M. Senila, and M. Stefan, "Removal of lead(II), cadmium(II), and arsenic(III) from aqueous solution using magnetite nanoparticles prepared by green synthesis with Box–Behnken design," *Analytical Letters*, vol. 51, no. 16, pp. 2519–2531, 2018.

[53] K. Al-Essa, "Heavy metals adsorption from aqueous solutions onto unmodified and modified Jordanian kaolinite clay: batch and column techniques," *American Journal of Applied Chemistry*, vol. 6, no. 1, p. 25, 2018.

[54] M. P. Das and L. J. Rebecca, "Removal of lead(II) by phyto-inspired iron oxide nanoparticles," *Nature Environment and Pollution Technology*, vol. 17, pp. 569–574, 2018.

[55] Y. Abshirini, H. Esmaeili, and R. Foroutan, "Enhancement removal of Cr (VI) ion using magnetically modified MgO nanoparticles," *Materials Research Express*, vol. 6, no. 12, article 125513, 2019.

[56] A. Sebastian, A. Nangia, and M. N. V. Prasad, "A green synthetic route to phenolics fabricated magnetite nanoparticles from coconut husk extract: implications to treat metal contaminated water and heavy metal stress in _Oryza sativa_ L," *Journal of Cleaner Production*, vol. 174, pp. 355–366, 2018.

[57] M. Ji, X. Su, Y. Zhao et al., "Effective adsorption of Cr(VI) on mesoporous Fe-functionalized Akadama clay: optimization, selectivity, and mechanism," *Applied Surface Science*, vol. 344, pp. 128–136, 2015.

[58] S. Venkateswarlu and M. Yoon, "Rapid removal of cadmium ions using green-synthesized Fe_3O_4nanoparticles capped with diethyl-4-(4 amino-5-mercapto-4H-1,2,4-triazol-3-yl)phenyl phosphonate," *RSC Advances*, vol. 5, no. 80, pp. 65444–65453, 2015.

[59] Z. Dahaghin, H. Z. Mousavi, and M. Sajjadi, "Synthesis and application of a novel magnetic SBA-15 nanosorbent for heavy metal removal from aqueous solutions," *Journal of Sol-Gel Science and Technology*, vol. 86, no. 1, pp. 217–225, 2018.

[60] W. Zhu, J. Wang, D. Wu et al., "Investigating the heavy metal adsorption of mesoporous silica materials prepared by microwave synthesis," *Nanoscale Research Letters*, vol. 12, no. 1, p. 323, 2017.

[61] H. Vatandoust, H. Younesi, Z. Mehraban, A. Heidari, and H. Khakpour, "Comparative adsorption of Cd (II) and Pb (II) by MCM-48 and amine-grafted MCM-48 in single and binary component systems," *Water Conservation Science and Engineering*, vol. 6, no. 2, pp. 67–78, 2021.

[62] L. P. Lingamdinne, K. R. Vemula, Y. Y. Chang, J. K. Yang, R. R. Karri, and J. R. Koduru, "Process optimization and modeling of lead removal using iron oxide nanocomposites generated from bio-waste mass," *Chemosphere*, vol. 243, article 125257, 2020.

[63] I. Ali, C. Peng, and I. Naz, "Removal of lead and cadmium ions by single and binary systems using phytogenic magnetic nanoparticles functionalized by 3-marcaptopropanic acid," *Chinese Journal of Chemical Engineering*, vol. 27, no. 4, pp. 949–964, 2019.

[64] P. K. Gautam, S. Shivalkar, and S. Banerjee, "Synthesis of _M. oleifera_ leaf extract capped magnetic nanoparticles for effective lead [Pb (II)] removal from solution: kinetics, isotherm and reusability study," *Journal of Molecular Liquids*, vol. 305, article 112811, 2020.

[65] A. T. Khadim, T. M. Albayati, and N. M. Cata Saady, "Desulfurization of actual diesel fuel onto modified mesoporous material Co/MCM-41. Environmental Nanotechnology," *Monitoring & Management*, vol. 17, article 100635, 2022.

[66] J. Shi, H. Li, H. Lu, and X. Zhao, "Use of carboxyl functional magnetite nanoparticles as potential sorbents for the removal of heavy metal ions from aqueous solution," *Journal of Chemical & Engineering Data*, vol. 60, no. 7, pp. 2035–2041, 2015.

[67] Y. Bagbi, A. Sarswat, D. Mohan, A. Pandey, and P. R. Solanki, "Lead (Pb2+) adsorption by monodispersed magnetite nanoparticles: surface analysis and effects of solution chemistry," *Journal of Environmental Chemical Engineering*, vol. 4, no. 4, pp. 4237–4247, 2016.